HiSST: 2nd International Conference on
High-Speed Vehicle Science & Technology
11–15 September 2022, Bruges, Belgium

Adjusting Transpiration Cooling to Real Time Surface Heat Flux Estimation

Fabian Hufgard[1], Christian Duernhofer[2], Stefan Loehle[3], Sven Schweikert[4], Clemens Mueller[5], Giuseppe di Martino[6], Hannah Boehrk[7], Johan Steelant[8], Stefanos Fasoulas[9]

Abstract

We present a new approach in theory and experiment to automatically adjust the transpiration cooling to the actual thermal load, i.e. the Cooling Adjustment for Transpiration Systems (CATS). This approach bases on the real-time determination of surface heat flux at the transpiration cooled wall. The heat flux is essentially calculated from a non-intrusive measurement of pressure in the plenum, i.e. the region between mass flow controller and porous wall. This pressure heat flux transformation additionally attenuates a destabilizing positive feedback loop, where the transpiration cooling controller's output (i.e. mass flow rate) strongly influences its input (i.e. plenum pressure). We describe the identification of the model parameters for the heat flux determination, which are found and verified by a calibration approach. CATS was demonstrated in the plasma wind tunnel PWK4 at the Institute of Space Systems, Stuttgart. The results show the CATS performance, which proves the usefulness of the proposed approach to automatically adjust the transpiration cooling to the actual thermal load.

Keywords: *transpiration cooling, porous material, heat flux, automatic adjustment, plasma wind tunnel*

Nomenclature

Latin

A – Area
a – Model parameter
b – Model parameter
c – Model parameter
c_p – Heat capacity
h_v – Volumetric heat transfer coefficient
K_D – Darcy permeability coefficient
K_F – Forchheimer permeability coefficient
L – Porous sample thickness
$\dot{m}$ – Mass flow rate
p – Pressure

[1]*PhD student, High Enthalpy Flow Diagnostics Group (HEFDiG), Institute of Space Systems, Pfaffenwaldring 29, 70569 Stuttgart, Germany, hufgard@irs.uni-stuttgart.de*
[2]*PhD student, High Enthalpy Flow Diagnostics Group (HEFDiG), Institute of Space Systems, Pfaffenwaldring 29, 70569 Stuttgart, Germany, cduernhofer@irs.uni-stuttgart.de*
[3]*Research scientist, Group leader HEFDiG, Institute of Space Systems, Pfaffenwaldring 29, 70569 Stuttgart, Germany, loehle@irs.uni-stuttgart.de*
[4]*Trumpf GmbH, Johann-Maus-Straße 2, 71254 Ditzingen, Germany, previously: PhD student, Institute of Aerospace Thermodynamics, Pfaffenwaldring 31, 70569 Stuttgart, Germany, sven.schweikert@trumpf.com*
[5]*M.Sc. student, High Enthalpy Flow Diagnostics Group (HEFDiG), Institute of Space Systems, Pfaffenwaldring 29, 70569 Stuttgart, Germany, clemens.hector@gmail.com*
[6]*Research scientist, High Temperature Management for Hypersonic Flight, DLR, Pfaffenwaldring 38-40, 70569 Stuttgart, Germany, giuseppe.dimartino@dlr.de*
[7]*Professor, Duale Hochschule Baden-Württemberg Stuttgart, Jaegerstrasse 58, 70174 Stuttgart, Germany, previously: Group leader High Temperature Management for Hypersonic Flight, DLR, hannah.boehrk@dhbw-stuttgart.de*
[8]*Senior research scientist, Flight Vehicles and Aerothermodynamics Engineering Section, ESA-ESTEC, Keplerlaan 1, P.O. Box 299, 2200 AG Noordwijk, Netherlands, johan.steelant@esa.int*
[9]*Professor, Director Institute of Space Systems, Pfaffenwaldring 29, 70569 Stuttgart, Germany, fasoulas@irs.uni-stuttgart.de*

Pos – Probe position in PWK experiment
$\dot{q}$ – Surface heat flux
R – Specific gas constant for an ideal gas
T – Temperature
t – Time
v – Darcy velocity
V – Volume
x – Spatial variable

Greek
λ – Thermal conductivity
μ – Dynamic viscosity
ρ – Density
Φ – Porosity

Subscripts
∞ – Ambient
det – Determined
eff – Effective property for porous material
f – Fluid
fc – Flow controller
in – Input
pl – Plenum
ps – Porous sample
s – Solid
set – Set point

1. Introduction

Transpiration cooling is an active thermal protection technique for aerospace applications [1–3]. Here a gaseous or liquid coolant is fed through a porous wall into the hot gas region. This has two effects. Firstly, the wall is actively cooled by the coolant itself [4]. Secondly, the coolant mixes into the boundary layer and by that reduces the boundary layer temperature, leading to a lower convective surface heat flux [1, 5, 6]. Both effects are boosted when increasing the coolant mass flow rate [1, 5–7]. However, a high mass flow rate also produces undesirable effects. A large coolant consumption necessitates a large coolant supply, thus more vehicle mass and volume. Also, the vehicle's drag increases with mass flow rate, which might be disadvantageous when it comes to sharp leading edges [8]. It furthermore triggers the onset of boundary layer transition earlier and shortens its extend resulting downstream in overshoots and higher heat transfer rates. Ideally the coolant mass flow rate is adjusted during flight to a level that is optimal for the actual thermal load. In order to achieve this, we developed the Cooling Adjustment for Transpiration Systems (CATS) technology. This technology will be tested in the HIFLIER1 flight experiment, scheduled in June 2023 [9]. CATS utilizes the correlation of surface heat flux and plenum pressure, which is subject to earlier studies by the authors [10–16]. Essentially, the plenum pressure is a measure for surface heat flux and the coolant mass flow rate is adjusted by the CATS controller accordingly.

2. Theoretical Approach

Consider a transpiration cooling system as sketched in Fig. 1. The pressure gradient over the porous wall is given by the Darcy-Forchheimer equation

$$p_{ps}(x,t)\frac{\partial p_{ps}(x,t)}{\partial x} = \frac{\mu_f(x,t)\,\dot{m}_{ps}(t)\,R\,T_f(x,t)}{K_D\,A} + \frac{\dot{m}_{ps}(t)^2\,R\,T_f(x,t)}{K_F\,A^2} \qquad 0 < x < L, \quad t \geq 0 \tag{1}$$

Integration of Eq. (1) over x and the introduction of the plenum pressure p_{pl} at $x = L$ and the constant ambient pressure p_∞ at $x = 0$ we obtain

$$\frac{p_{pl}^2(t) - p_\infty^2}{2} = \int_0^L \left(\frac{\mu_f(x,t)\,\dot{m}_{ps}(t)\,R\,T_f(x,t)}{K_D\,A} + \frac{\dot{m}_{ps}^2(t)\,R\,T_f(x,t)}{K_F\,A^2} \right) dx \qquad t \geq 0 \tag{2}$$

The interaction of surface heat flux and plenum pressure is analyzed in more detail in e.g. [13]. In simple terms, a heat flux to the surface will increase the temperature of the porous wall and the fluid therein, which according to Eq. (2) will eventually lead to an increased plenum pressure. This means that one can determine the surface heat flux from measurement of the plenum pressure. Using this surface heat flux information, one can adjust the mass flow rate in order to boost the transpiration cooling performance. The main difficulty is that the adjustment of the mass flow rate also causes a plenum pressure rise. This results in a positive feedback loop on the plenum pressure, which leads to instability. For this reason

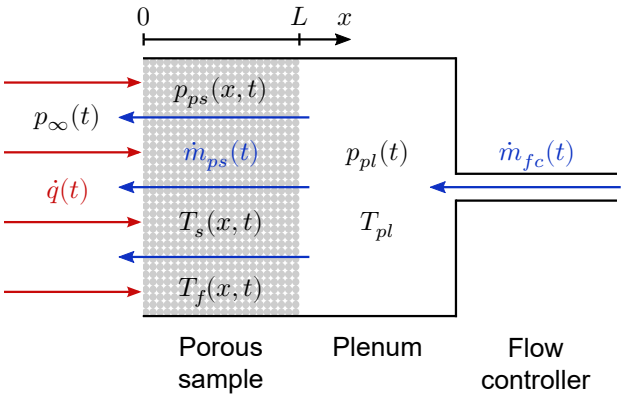

Fig. 1. Schematic of a transpiration cooling system

one can not simply usefully utilize the plenum pressure signal directly as the input into a controller to adjust transpiration cooling. In this section we derive a new approach to circumvent this difficulty. Essentially, this approach enables us to process the plenum pressure in real time into surface heat flux. This heat flux signal is used as the input into a simple proportional controller which adjusts the setpoint of the mass flow controller (MFC). We call this approach Cooling Adjustment for Transpiration Systems (CATS).

The energy equations for solid (3a) and fluid (3b) in a transpiration cooled porous wall are given by [4]

$$(1-\Phi)\,\rho_s\,c_{p,s}\,\frac{\partial T_s(x,t)}{\partial t} = (1-\Phi)\,\lambda_s\,\frac{\partial^2 T_s(x,t)}{\partial x^2} - h_v\,\left(T_s(x,t)-T_f(x,t)\right) \quad 0<x<L,\ t\geq 0 \tag{3a}$$

$$\Phi\,\rho_f\,c_{p,f}\left(\frac{\partial T_f(x,t)}{\partial t} + v(t)\frac{\partial T_f(x,t)}{\partial x}\right) = \Phi\,\lambda_f\frac{\partial^2 T_f(x,t)}{\partial x^2} + h_v\,\left(T_s(x,t)-T_f(x,t)\right) \quad 0<x<L,\ t\geq 0 \tag{3b}$$

with time t, the spatial variable x, the temperature T, thermal conductivity λ, density ρ, specific heat capacity c_p, the volumetric heat transfer coefficient h_v, the Darcy velocity v, the porosity Φ and the porous wall cross section A. The subscripts $(_s)$ and $(_f)$ assign the variables to the solid and fluid respectively. Solving both equations for $h_v\,\left(T_s(x,t)-T_f(x,t)\right)$ allows to join Eqs. (3a) and (3b) into the following single equation.

$$\rho_{s,eff}\,c_{p,s}\,\frac{\partial T_s(x,t)}{\partial t} + \Phi\,\rho_f\,c_{p,f}\,\frac{\partial T_f(x,t)}{\partial t} + \frac{\dot{m}_{ps}(t)\,\Phi\,c_{p,f}}{A}\,\frac{\partial T_f(x,t)}{\partial x} = \lambda_{s,eff}\,\frac{\partial^2 T_s(x,t)}{\partial x^2} \tag{4}$$

Here, we neglect conduction through the fluid and substitute the Darcy velocity with $v=\dot{m}_{ps}/\rho_f\,A$. We substituted the effective material properties $\rho_{s,eff}=(1-\Phi)\,\rho_s$ and $\lambda_{s,eff}=(1-\Phi)\,\lambda_s$. Since we intent to adjust the mass flow rate through the MFC $\dot{m}_{fc}(t)$, the mass flow rate through the porous sample $\dot{m}_{ps}(t)$ is also a function of time. Assuming local thermal equilibrium (LTE), i.e. $T_f(x,t)=T_s(x,t)=T(x,t)$, substitution of the heat flux within the porous wall $-\dot{q}_{ps}=\lambda_{s,eff}\,\partial T/\partial x$ in the right side of the equation and substitution of $\rho_f=p/RT$ yields

$$\left(\rho_{s,eff}\,c_{p,s}+\Phi\,\frac{p_{ps}(x,t)}{RT(x,t)}\,c_{p,f}\right)\,\frac{\partial T(x,t)}{\partial t} + \frac{\dot{m}_{ps}(t)\,\Phi\,c_{p,f}}{A}\,\frac{\partial T(x,t)}{\partial x} = -\frac{\partial \dot{q}_{ps}(x,t)}{\partial x} \tag{5}$$

with the pressure in the porous wall $p_{ps}(x,t)$ and specific gas constant for an ideal gas R. Simplifying Eq. (5) by assuming a lumped wall gives an equation to determine the surface heat flux:

$$\left(\rho_{s,eff}\,c_{p,s}+\Phi\,\frac{\bar{p}_{ps}(t)}{R\bar{T}(t)}\,c_{p,f}\right)\,L\,\frac{d\bar{T}(t)}{dt} + \frac{\dot{m}_{ps}(t)\,\Phi\,c_{p,f}}{A}\,\left(\bar{T}(t)-T_{pl}\right) = \dot{q}(t) \tag{6}$$

with the lumped wall temperature $\bar{T}(t)$, the mean fluid pressure in the porous wall $\bar{p}_{ps}(t)$, the length of the porous wall L, the surface heat flux $\dot{q}_{ps}(x=0,t)=\dot{q}(t)$ and the assumptions that the back wall is adiabatic, i.e. $\dot{q}_{ps}(x=L,t)=0$, and the inbound fluid temperature equals the fluid temperature in the plenum T_{pl}, which is constant, i.e. $T(x=L,t)=T_{pl}=const.$.

The required time dependent variables in Eq. (6) are $\bar{p}_{ps}(t)$, $\dot{m}_{ps}(t)$ and $\bar{T}(t)$. The variables $\bar{p}_{ps}(t)$ and $\dot{m}_{ps}(t)$ are given by

$$\bar{p}_{ps}(t) = \frac{2}{3}\,\frac{p_{pl}^3(t)-p_{\infty}^3(t)}{p_{pl}^2(t)-p_{\infty}^2(t)} \tag{7}$$

$$\dot{m}_{ps}(t) = \dot{m}_{fc}(t) - \frac{V_{pl}}{R\,T_{pl}}\frac{dp_{pl}(t)}{dt} \tag{8}$$

with the plenum volume V_{pl} and $\bar{T}(t)$ can be found by solving the Darcy equation for

$$\mu(t)\,\bar{T}(t) = \frac{p_{pl}^2(t)-p_{\infty}^2(t)}{2}\,\frac{K_D\,A}{\dot{m}_{ps}(t)\,R\,L} \quad . \tag{9}$$

The product $\mu(t)\,\bar{T}(t)$ is a bijective function of $\bar{T}$ when approximating the fluid viscosity $\mu(t)$ using Sutherland's Law. We implemented this calculation of $\bar{T}$ using a simple look-up table. K_D is the porous material's permeability coefficient. We do not use the Darcy-Forchheimer equation to solve for $\bar{T}$, because K_F is orders of magnitude bigger than K_D and $\dot{m}_{ps}$ is quite small, which results in a negligible Forchheimer term.

Eqs. (7) to (9) require input of the variables $p_{pl}(t)$, $p_{\infty}(t)$, $\dot{m}_{fc}(t)$ and T_{pl}, which are measured during a given experiment. Note that the determination of surface heat flux requires these four measurements as input, which are exclusively non-intrusive. No particular sensor must be equipped inside the porous wall itself and the coolant flow through the porous wall is therefore not disturbed. In addition, these calculations are computationally relatively cheap, which enables the heat flux determination in quasi real-time.

For simplicity, we merge the constant parameters in Eq. (6) into the parameters

$$a = \rho_{s,eff}\,c_{p,s}\,L \tag{10a}$$

$$b = \frac{\Phi\,c_{p,f}\,L}{R} \tag{10b}$$

$$c = \frac{\Phi\,c_{p,f}}{A} \tag{10c}$$

and yield

$$\dot{q}(t) = a\,\frac{d\bar{T}(t)}{dt} + b\,\frac{\bar{p}_{ps}(t)}{\bar{T}(t)}\,\frac{d\bar{T}(t)}{dt} + c\,\dot{m}_{ps}(t)\left(\bar{T}(t)-T_{pl}\right) \tag{11}$$

Equation (11) enables the real-time determination of surface heat flux. The model parameters a, b and c can be calculated from material properties and geometry data using Eqs. (10). Accounting for the simplifications and assumptions made in the derivation of Eq. (11), this form enables us to calibrate the model parameters for the given transpiration cooling system. This calibration approach is detailed in subsection 4.2.

Based on the real-time determination of heat flux using Eq. (11), the CATS controller automatically adjusts the set point of mass flow rate at the MFC $\dot{m}_{fc,set}$ by

$$\dot{m}_{fc,set} = \dot{m}_{fc,0} + \dot{q}\cdot\frac{\dot{m}_{fc,max}-\dot{m}_{fc,0}}{\dot{q}_{max}} \tag{12}$$

with the initial mass flow rate $\dot{m}_{fc,0}$, the MFC's maximum mass flow rate $\dot{m}_{fc,max}$ and the maximum expected heat flux $\dot{q}_{max}$. The CATS controller in our system acts as a p-controller with the proportional

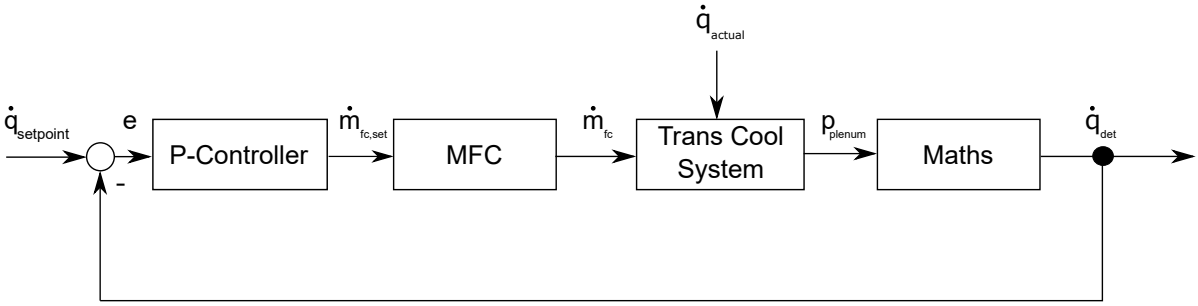

Fig. 2. Layout of CATS

gain $k_p = (\dot{m}_{fc,max} - \dot{m}_{fc,0}) / \dot{q}_{max}$ and the offset $\dot{m}_{fc,0}$ (cf. Eq. (12)). The resulting CATS layout is summarized in Fig. 2. Here, we define the set point $\dot{q}_{setpoint} = 0$.

To summarize the theoretical approach, CATS is a technology to automatically adjust the transpiration cooling where the required measurement inputs are exclusively non-intrusive. The prime feature of CATS is that it reacts to the surface heat flux rather than time delayed quantities as e.g. wall temperature. This boosts the protective characteristic of the transpiration cooling technique in the same instance the actual heating affects the surface. This minimizes the total heating of the wall. In theory, the proposed pressure heat flux transformation eliminates a destabilizing positive feedback loop, where the controller output - mass flow rate - significantly influences its input - plenum pressure.

3. Transpiration Cooling System

The complete transpiration cooling system that was used for both calibration and PWK experiments is shown in Fig. 3. It consists of the sensor head, a pressure gauge, a MFC and respective tubing between the components.

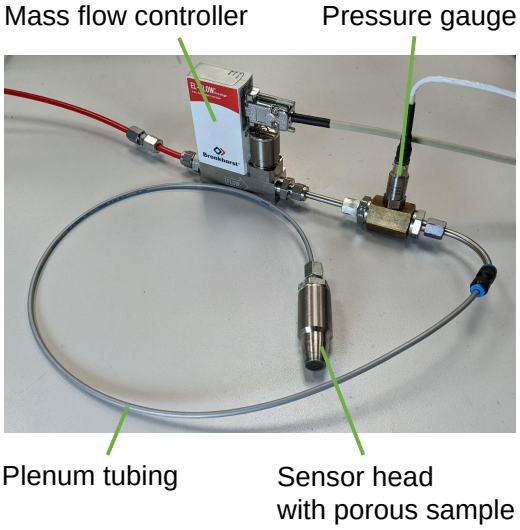

Fig. 3. The transpiration cooling system

A schematic and a macro photo of the sensor head is shown in Figure 4. The porous sample is made of carbon/carbon (C/C). It was manufactured and characterized by the German Aerospace Center (DLR) in Stuttgart. The C/C sample was machined into a truncated conical shape with a draft angle of $10°$ and a front diameter of 10.6 mm (smaller diameter of truncated cone). With a sample length L of 7.5 mm follows

a mean sensor diameter of 11.5 mm and a mean cross section A of $1.1 \cdot 10^{-4}$ m^2. The Darcy permeability coefficient K_D for the porous sample in this study was determined to be about $4 \cdot 10^{-13}$ m^2. The porous sample is pressed into a titanium housing by a set screw. A spring accounts for thermal expansion. A Sigraflex graphite foil acts as the sealant between porous sample and housing. The sensor head's total length including the shown connector screw is 81 mm and its maximum diameter is 25 mm.

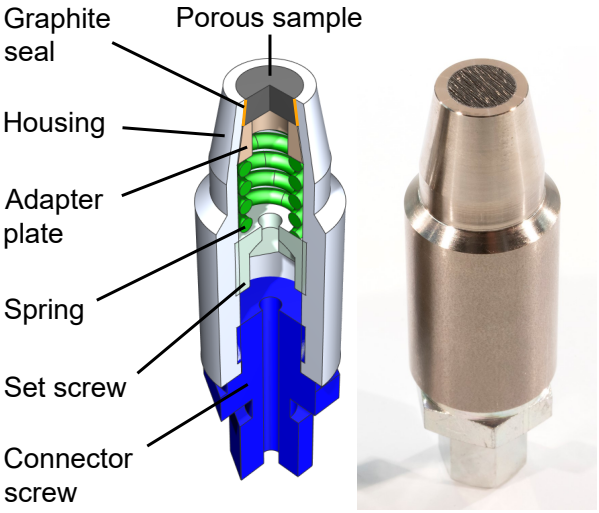

Fig. 4. Transpiration cooling sensor head schematic (left) and photo (right)

A thin tube leads from the connector screw at the back of the sensor head to the pressure gauge and the MFC. The pressure gauge is a *Kulite ETQ-12-375M-5BARA* with an accuracy of 0.6%. The MFC is a *Bronkhorst FG-201CV-AAD-33-V-AA-000* with a range of $0 - 40$ mg/s and an accuracy of 0.6%. The MFC is supplied with nitrogen with a constant pressure of 16 bar. The total plenum volume V_{pl} was determined to $15.0 \cdot 10^{-6}$ m^3 for the calibration measurements. The tubing had to be slightly modified for the PWK experiments resulting in a plenum volume of $15.7 \cdot 10^{-6}$ m^3 in the PWK measurement.

4. Calibration and Verification

The aim of the calibration stage is to fine tune and verify the heat flux determination model given by Eq. 11. We did the parameter tuning in two steps: first we fit the model parameters a, b and c to measurement data from an experiment with CATS in open-loop mode, i.e. we establish a constant $\dot{m}_{fc}$ without feeding the CATS output back into the MFC. In the second step we fine tuned the found model parameters for CATS in closed loop mode. Here we took care to obtain both an accurate heat flux determination and a stable CATS controller. In this section we describe the experimental setup for the calibration experiments, the calibration of the heat flux determination model and closed loop verification.

4.1. Experimental Setup for Calibration and Verification

The experimental setup for calibration and verification is shown in the left photo in Figure 5. The well-characterized heat flux is provided by a *Laserline LDM 500-100* diode laser with a wavelength of 910 nm and a power rise time of < 0.1 ms. The focusing optics in the laser head expand the laser beam homogeneously into a square-shaped spot, which is illustrated for our setup in the right photo in Figure 5. In order to minimize lateral conduction, the radiated area slightly overlapped the porous material's surface to all sides.

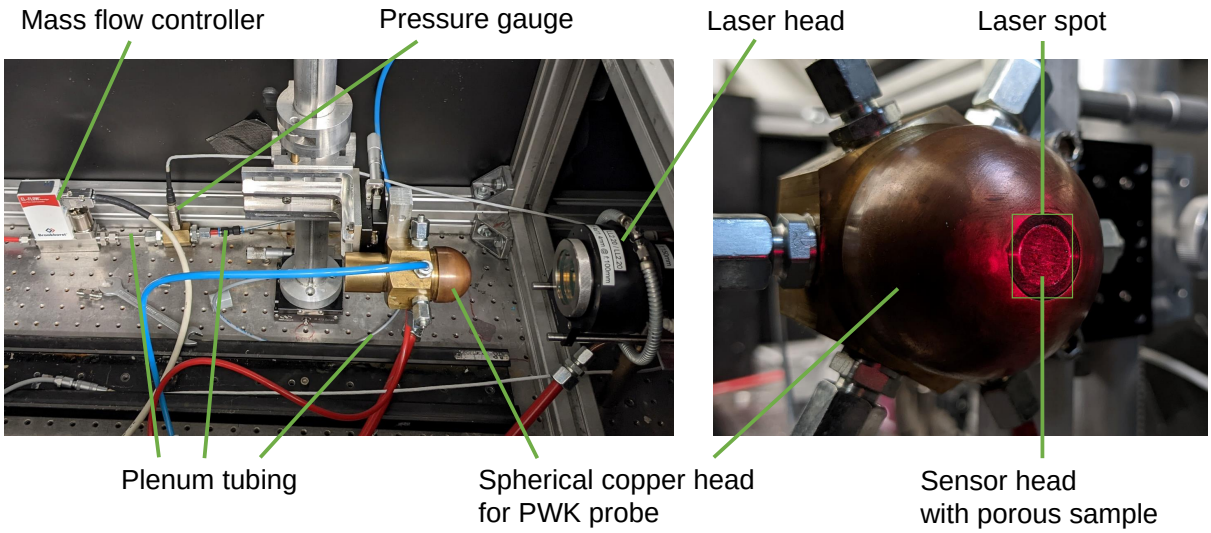

Fig. 5. Experimental setup for calibration (left) and visual impression of laser spot on transpiration cooled sensor surface (right)

4.2. Calibration of Heat Flux Estimation Model

The data of the heat flux determination model calibration are shown in Fig. 6. In this experiment, we established a constant mass flow rate set point $\dot{m}_{fc,set}$ and applied an arbitrary heat flux using the diode laser. The laser's output power is recorded and calculated into the net surface heat flux $\dot{q}_{in}$. We measured the plenum pressure $p_{pl}(t)$, and the actual value of mass flow rate through the MFC $\dot{m}_{fc}$, which consequently equals the constant set point, i.e. $\dot{m}_{fc} = \dot{m}_{fc,set}$. The ambient pressure $p_\infty = 0.9545$ bar and the plenum temperature $T_{pl} = 295$ K remained fairly constant over the course of all calibration experiments. With these measurements, we calculate $\bar{p}_{ps}$, $\dot{m}_{ps}$ and $\bar{T}$ using Eqs. (7) to (9) and the look-up table as described in section 2. The temperature's time derivative $d\bar{T}/dt$ is calculated at each time step n_t using the two-point backward difference $d\bar{T}/dt(n_t) = (T(n_t) - T(n_t - 1))/\Delta t$ with the time step width Δt. The time step width was $\Delta t = 80$ ms in all experiments.

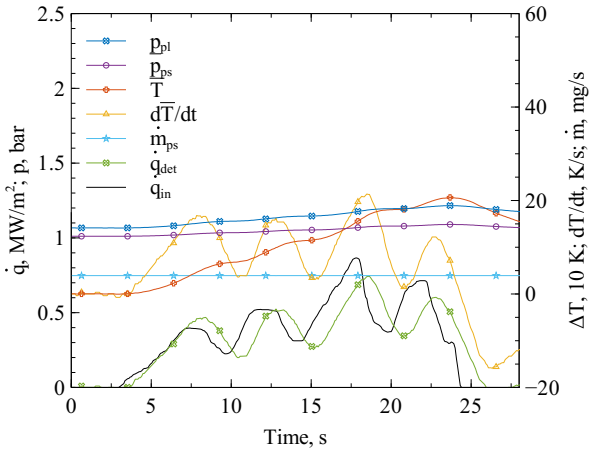

Fig. 6. Experimental data for calibration of heat flux determination model

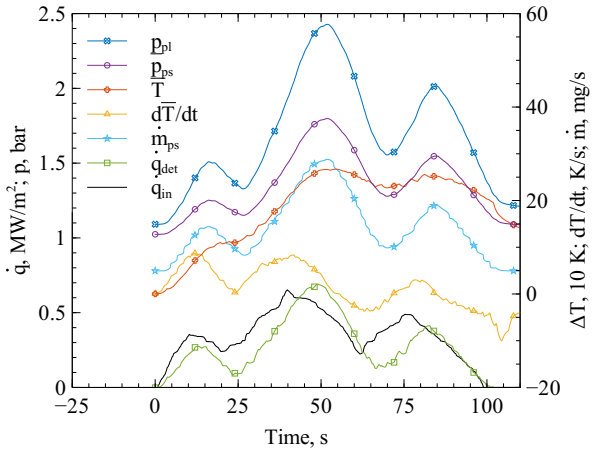

Fig. 7. Closed loop verification data with real-time determined heat flux

Using the data shown in Fig. 6, the model parameters a, b and c were fitted to Eq. (11). As a starting point for the fit, we calculated the model parameters using the analytical expressions from Eqs. (10) and the material and geometry data summarized in table 1. Both the parameter fit and the analytical values are given in table 2.

Table 1. Material and geometry data of the porous C/C sample and nitrogen

Φ	$\rho_{s,eff}$	$c_{p,s}$	$c_{p,f}$	R	L	A
12,4% [17]	$1400\,\mathrm{kg/m^3}$ [3]	$1650\,\mathrm{J/(kg\,K)}$ [3]	$1040\,\mathrm{J/(kg\,K)}$	$297\,\mathrm{J/(kg\,K)}$	$7.5\,\mathrm{mm}$	$1.11\,\mathrm{cm^2}$

Table 2. Model parameters for different measurement scenarios

	a	b	c
Analytical value	$1.7 \cdot 10^4$	$3.3 \cdot 10^{-3}$	$1.2 \cdot 10^6$
Model calibration	$1.6 \cdot 10^4$	22	$4.4 \cdot 10^8$
Closed loop validation	$1.6 \cdot 10^4$	15	$8 \cdot 10^7$
PWK experiment	$1.0 \cdot 10^4$	10	$4 \cdot 10^7$

As can be seen in Fig. 6, the heat flux determination $\dot{q}_{det}$ matches the input heat flux $\dot{q}_{in}$ fairly well, but time delayed. The time delayed reaction of the two signals may be explained by the introduction of moving average filters to the signals of p_{pl}, dp_{pl}/dt, $d\bar{T}/dt$ and $\dot{m}_{fc,set}$ with the widths 4, 154, 47 and 41 data points which amounts to a length of 0.3, 12.3, 3.8 and $3.3\,\mathrm{s}$ respectively. Especially the filter for dp_{pl}/dt is quite broad-ranged. These filters were introduced in order to stabilize the CATS controller.

4.3. Closed Loop Verification

The aim of the closed loop verification was to verify the found model parameters for the active closed loop CATS controller. Here, the set point of the MFC is adjusted by CATS. Since the mass flow rate effects the plenum pressure and the plenum pressure is at the same time an essential input of CATS, the system is a positive feedback loop controller. In theory this feedback loop is eliminated by the approach described in section 2, but we observed that the system still tends to instability with the calibration model parameters. The reason for the instability might be a difference in time delay through filtering of the signals for $\bar{T}$ and $\dot{m}_{ps}$, where the $\bar{T}$ signal is in total subject to broader filters and thus more time delayed. These terms play a role in last term in Eq. (11), which is the term for energy loss through hot gas motion. For a given heat flux and a rising $\dot{m}_{ps}$, the temperature difference $\bar{T} - T_{pl}$ decreases. If that decrease is time delayed with respect to $\dot{m}_{ps}$, the heat flux is overestimated resulting in a positive feedback loop. The same applies to the second term in Eq. 11. In order to reduce this effect and achieve a stable controller, we modified the model parameters b and c slightly. Here we took care to maintain an accurate heat flux determination.

Figure 7 shows a verification experiment with the closed loop controller, where we used the modified model parameters given in table 2. As one can see, the system remains stable in this experiment and the heat flux determination $\dot{q}_{det}$ matches the input heat flux $\dot{q}_{in}$ fairly well. The determined heat flux shows a similar time delay as in the model calibration (cf. Fig.6) and is also explained by the introduced filters discussed in subsection 4.2. CATS adjusts the mass flow rate set point $\dot{m}_{fc,set}$, which reflects in the mass flow rate through the porous sample $\dot{m}_{ps}$. As a consequence, the plenum pressure rises, because more pressure is required to press the coolant through the porous sample at an increased rate. We conclude from this that CATS works in the laser setup for the given model parameters (see table 2).

Comparing the calibration measurement (Fig. 6) and the closed loop measurement (Fig. 7), illustrates the effect of the positive feedback loop on the plenum pressure. The actual plenum pressure change

that arises from the surface heat flux is roughly an order of magnitude weaker than the plenum pressure change due to the adjustment of mass flow rate. This significantly aggravates a controller relying on the plenum pressure as the control parameter and at the same time promotes the value of the proposed approach, where the positive feedback loop is damped.

5. Plasma Wind Tunnel Experiment

CATS was tested in the plasma wind tunnel PWK4 at the Institute of Space Systems, Stuttgart. In this section we describe the setup for these experiments, the flow characteristics and the results.

5.1. Experimental Setup for Plasma Wind Tunnel Experiment

The experimental setup of the PWK4 test is shown in Figure 8. The sensor head is mounted into the tip of the PWK probe. The sensor head was integrated into the same copper half sphere as in the calibration setup. The transpiration cooled surface orientation opposes the plasma flow direction. The tube from the back of the sensor head leads through the interior of the PWK probe to the pressure gauge. The pressure gauge and the MFC are located beneath the movable platform.

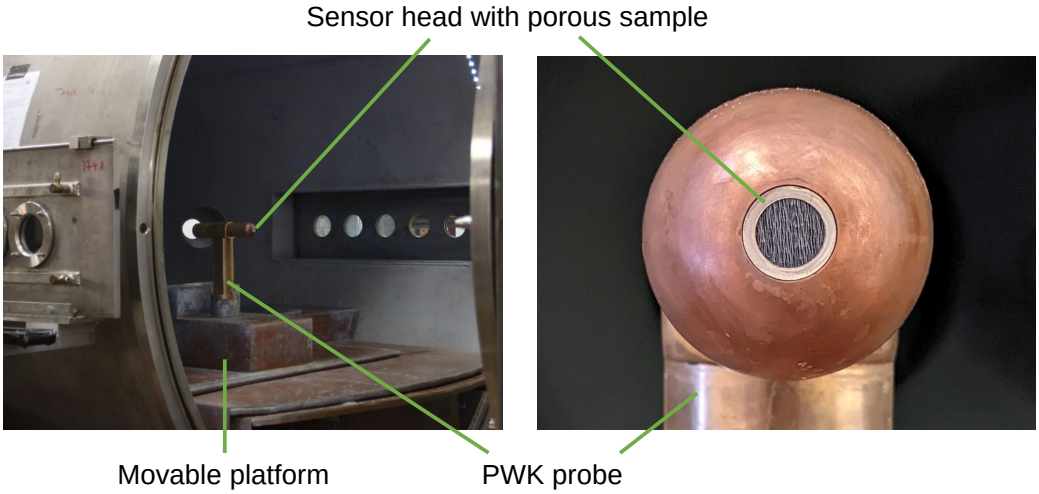

Fig. 8. Experimental setup for plasma wind tunnel tests (left) and close up photo of probe head (right)

5.2. Plasma wind tunnel flow condition

The characteristics of the flow condition are summarized in table 3. The ambient pressure that the transpiration cooling system is exposed to changes during the course of the experiment. Initially the ambient pressure equals the tank pressure of $p_{tank} = 52\,\text{Pa}$ and increases up to roughly $1250\,\text{Pa}$ in the plasma flow's stagnation point. This variation is not measured and thus accounted for in the experiments. However, this ambient pressure variation is rather small, when compared to the development of plenum pressure, which is $> 32000\,\text{Pa}$. Considering the fact that the pressure variables are squared or cubed in Eqs. (7) and (9), this effect of the ambient pressure variation is ruled negligible. For this reason, the ambient pressure was assumed to remain constant.

Table 3. Test condition of the PWK4 experiment

I	U	p_{tank}	$\dot{m}_{ges}$	I_{mag}
$604\,\text{A}$	$90\,\text{V}$	$52\,\text{Pa}$	$6.52\,\text{g/s}$	$100\,\text{A}$

5.3. Results of Plasma Wind Tunnel Experiment

Figure 9 shows the results of the CATS demonstration in the PWK4. The change of the axial Pos_{axial} and radial position Pos_{radial} indicate the movement of the probe in the PWK4. During startup, the probe was positioned outside the plasma jet at a distance to the generator nozzle of 490 mm. Once the flow condition was set, the probe was first moved in radial direction into the plasma jet center. After a short time, the probe was moved axially towards the plasma generator up to a distance of 90 mm. During the axial movement the probe remained in the plasma flow's stagnation point. Finally, the probe was moved radially out of the jet.

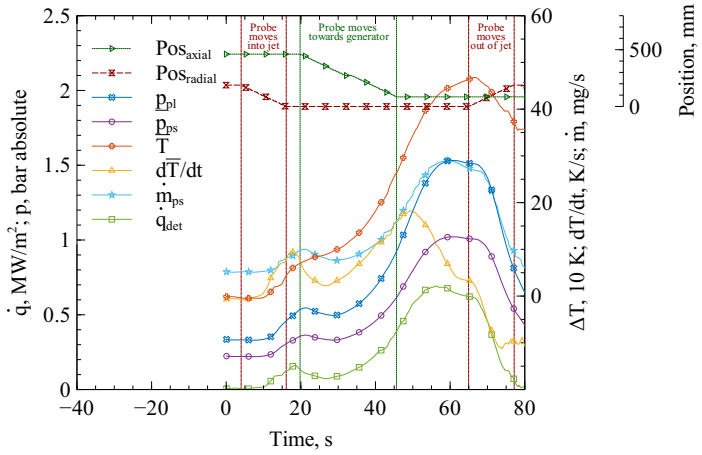

Fig. 9. Demonstration of CATS in plasma wind tunnel PWK4 experiment

Moving in radial direction into the jet leads to a heat flux increase onto the transpiration cooled surface. This is detected by CATS as can be seen from the rising signal of determined heat flux $\dot{q}_{det}$ during that phase (cf. Fig.9). The mass flow rate is adjusted accordingly, which reflects on the mass flow rate through the porous sample $\dot{m}_{ps}$. The surface heat flux is expected to increase during the axial movement towards the generator. This is also detected and the CATS controller automatically increases the mass flow rate. Between 46 s and 65 s, the probe remained in the same position which means a constant flow condition. CATS required about 10 s to stabilize to this constant flow condition, which is to be explained by the rather broad-ranging moving average filters introduced in the signal processing of CATS. However, the heat flux signal decreases after this stabilization period, which is an effect of the increased out blowing. We conclude from this that the demonstration of CATS was successful.

During previous PWK experiments, the found model parameters from the closed loop verification resulted in an unstable CATS controller. The model parameters were therefore adapted manually until the CATS showed stable behavior. The resulting parameters listed in table 2 were defined in the CATS settings during the experiment presented in Fig. 9. The adaption of the model parameters introduces an error of up to roughly 60% to the real time heat flux determination. Nevertheless, the CATS controller functioned qualitatively as desired.

6. Conclusion

This paper shows a new approach in theory and experiment to automatically adjust the cooling rate of a transpiration cooled wall depending on the actual surface heat flux. This boosts the protective characteristic of the transpiration cooling technique in the same instance the actual heating affects the surface. The proposed model requires the time variant inputs plenum and ambient pressure, mass flow rate through the mass flow controller and temperature of the inbound coolant temperature. All of these are non-intrusive measurements, thus the porous wall does not required to be equipped with any sensor. We calibrated and verified the model parameters for the determination of surface heat flux using an

infrared laser. A Cooling Adjustment for Transpiration Systems (CATS) controller was successfully tested in a plasma wind tunnel experiment. This is the first experimental proof of a controller to automatically adjust the transpiration cooling to the actual heat load.

7. Acknowledgements

This work is partly funded through the ESA NPI Program under contract No. 4000121220/17/NL/MH. The effort by Marcus Selzer of DLR, German Aerospace Center in Stuttgart regarding the validation of the sensor sealing is greatly acknowledged. The authors thank the members of the High Enthalpy Flow Diagnostics Group for their help with the PWK experiments and fruitful discussions.

References

[1] W. M. Kays. Heat transfer to the transpired turbulent boundary layer. *International Journal of Heat and Mass Transfer*, 15(5):1023–1044, 1972.

[2] David E. Glass, Arthur D. Dilley, and H. Neale Kelly. Numerical analysis of convection / transpiration cooling. *Journal of Spacecraft and Rockets*, 38(1):15–20, 2001.

[3] H. Boehrk, O. Piol, and M. Kuhn. Heat balance of a transpiration-cooled heat shield. *Journal of Thermophysics and Heat Transfer*, 24(3):581–588, 2010.

[4] Donald A. Nield and Adrian Bejan. *Convection in porous media*. Springer, New York, NY, 4. ed. edition, 2013.

[5] J. G. Marvin and R. B. Pope. Laminar convective heating and ablation in the mars atmosphere. *AIAA Journal*, 5(2):240–248, 1967.

[6] J. T. Howe. Hypervelocity atmospheric flight: Real gas flow fields.

[7] S. Schweikert. *Ein Beitrag Zur Beschreibung Der Transpirationskühlung an Keramischen Verbundwerkstoffen*. PhD thesis, Universität Stuttgart, Institut für Thermodynamik der Luft- und Raumfahrt, 2019.

[8] M. J. Bulman. Transpiration cooling for a vehicle with low radius leading edges, 1994.

[9] G. Di Martino, H. Boehrk, J. Schaefer, C. Mueller, J. Peichl, F. Hufgard, C. Duernhofer, and S. Loehle. Design of the transpiration cooled fin experiment finex ii on hiflier1. In *HiSST*, Brugge, BE, 2022.

[10] S. Loehle, S. Schweikert, and J. von Wolfersdorf. Method for heat flux determination of a transpiration cooled wall from pressure data. *Journal of Thermophysics and Heat Transfer*, 30(3):567–572, 2016.

[11] F. Hufgard, S. Loehle, T. Hermann, S. Schweikert, M. McGilvray, J. von Wolfersdorf, J. Steelant, and S. Fasoulas. Analysis of porous materials for transpiration cooled heat flux sensor development. In *HiSST*, Moscow, Russia, 2018.

[12] F. Hufgard, S. Loehle, J. von Wolfersdorf, S. Fasoulas, M. Ewenz Rocher, T. Hermann, M. McGilvray, and J. Steelant. Surface heat flux measurement in transpiration cooled porous materials using plenum pressure data. In *SciTech 2019*, Reston, VA, USA, 2019. AIAA.

[13] F. Hufgard, S. Loehle, M. McGilvray, T. Hermann, S. Schweikert, J. von Wolfersdorf, J. Steelant, and S. Fasoulas. Plenum pressure behavior in transiently heat loaded transpiration cooling system. *Journal of Thermophysics and Heat Transfer*, 35(2):256–267, 2021.

[14] F. Hufgard, S. Loehle, H. Boehrk, M. McGilvray, J. Steelant, and S. Fasoulas. A heat flux sensor based on transpiration cooling. In *HiSST*, Brugge, BE, 2022.

[15] F. Hufgard, S. Loehle, and S. Fasoulas. Heat flux determination from pressure data in transpiration cooling experiment. In *ICIPE*. 2022.

[16] F. Hufgard, C. Duernhofer, S. Fasoulas, and S. Loehle. A transpiration cooled heat flux sensor utilizing plenum pressure: Measurement in high enthalpy flow. In *FAR - 2nd International Conference on Flight Vehicles, Aerothermodynamics and Re-entry Missions & Engineering*, Noordwijk, The Netherlands, 2022. ESA Publications Division.

[17] M. Selzer, S. Schweikert, H. Boehrk, H. Hald, and J. von Wolfersdorf. Comprehensive c/c sample characterizations for transpiration cooling applications.